

Simulation of Three-Dimensional Bénard-Marangoni Flows Including Deformed Surfaces

Tormod Bjøntegaard and Einar M. Rønquist*

Department of Mathematical Sciences, Norwegian University of Science and Technology, N-7491 Trondheim, Norway.

Received 14 September 2007; Accepted (in revised version) 7 November 2007

Available online 1 August 2008

Abstract. We present a coupled thermal-fluid model for Bénard-Marangoni convection in a three-dimensional fluid layer. The governing equations are derived in detail for two reasons: first, we do not assume a flat free surface as commonly done; and second, we prepare for the use of flexible discretizations. The governing equations are discretized using spectral elements in space and an operator splitting approach in time. Since we are here primarily interested in steady state solutions, the focus is on the spatial discretization. The overall computational approach is very attractive to use for several reasons: (i) the solution can be expected to have a high degree of regularity, and rapid convergence can be expected; (ii) the spectral element decomposition automatically gives a convenient parameterization of the free surface that allows powerful results from differential geometry to easily be exploited; (iii) free surface deformation can readily be included; (iv) both normal and tangential stresses are conveniently accounted for through a single surface integral; (v) no differentiation of the surface tension is necessary in order to include thermocapillary effects (due to integration-by-parts twice); (vi) the geometry representation of the free surface need only be C^0 across element boundaries even though curvature effects are included. Three-dimensional simulation results are presented, including the free surface deflection due to buoyancy and thermocapillary effects.

AMS subject classifications: 65C20, 76D05, 76D45, 76E06, 65N35, 53A05

Key words: Benard-Marangoni, free surface flows, differential geometry, spectral elements.

1 Introduction

We consider here Bénard-Marangoni convection where a fluid layer is heated from below. This problem has previously been studied extensively experimentally, theoretically, and

*Corresponding author. *Email addresses:* bjontega@math.ntnu.no (T. Bjøntegaard), ronquist@math.ntnu.no (E. M. Rønquist)

computationally. One of the intriguing features with this problem is the formation of hexagonal convection cells from random initial conditions; see [2, 14, 25]. This formation can originate from different effects: it can be caused by small density variations due to the fact that the density is a function of the temperature (i.e., from buoyancy forces), or it can be due to variations in the surface tension due to the fact that the surface tension is a function of the temperature (i.e., thermocapillary forces), or both effects can be present at the same time.

However, the free surface deformation associated with these cells has previously only been studied experimentally [2, 6, 14] or analyzed analytically using linear stability analysis [23]. It is known experimentally that the free surface will either be depressed or elevated over each hexagonal cell, depending on whether surface-tension-gradient effects or buoyancy effects are dominating [14]. It should be remarked that Bénard himself had an incorrect interpretation of which effect was dominating in his original experiments [2]; Rayleigh's [22] subsequent stability analysis also assumed buoyancy-driven convection. Only several decades later were Bénard experiments correctly interpreted through surface-tension-gradient effects [4, 21, 23].

To our knowledge, the deflection of the free surface has never before been investigated using simulation tools; only a fixed and flat "free surface" has been used in earlier numerical studies [19, 24]. We assume that this is partially due to the fact that the free surface deformation is small, but also partially because the imposition of the simultaneous curvature and surface-gradient effects along curved boundaries is a non-trivial task.

Our goal with this study is to present a way to accurately simulate Bénard-Marangoni convection, including the free surface deformation. Our work will focus on the prediction of steady state solutions. The solutions (velocity, temperature, pressure, and geometry) are expected to be of high regularity, and thus high order spatial discretizations should be very attractive to use for this class of application.

The governing equations for this problem are the incompressible Navier-Stokes equations coupled to a convection-diffusion equation for the temperature. Because our goal is to impose general free surface boundary conditions on potentially deformed surfaces, we need to use the full stress formulation of the Navier-Stokes equations. This formulation is not commonly used in earlier analysis due to the simplified assumptions about a flat "free surface." In addition, similar to the approach presented in [12], we would like to represent the free surface boundary conditions in general curvilinear coordinates; this will prove very advantageous for the subsequent numerical treatment.

An outline of the paper is as follows. In Section 2 we present a derivation of the full mathematical model for Bénard-Marangoni convection. We present the governing equations in strong form, including all the boundary conditions, and allowing for all the possible effects discussed above. Since such a complete model is not commonly used, we present the derivation in some detail, including some important results from differential geometry. We also present the non-dimensionalization of the governing equations and introduce the relevant non-dimensional numbers for this problem. In Section 3 we present the weak formulation of the governing equations. In particular, we exploit the

powerful results presented in [12] that allow for a very convenient way to impose the free surface boundary conditions. In Section 4 we present the Arbitrary Lagrangian Eulerian (ALE) formulation of the governing equations, and this formulation represents the starting point for our discretization. In Section 5 we discuss a discretization approach based on spectral elements in space [17] and an operator splitting approach in time. However, the discussion is limited to particular aspects of the surface parameterization, and how to conveniently impose both the normal and tangential stresses along the free surface. We then present a numerical test problem in Section 6, followed by a number of simulation results of three-dimensional Bénard-Marangoni convection in Section 7.

2 Governing equations: Strong form

We consider Bénard-Marangoni convection problem in a three-dimensional container including both buoyancy-driven flows (natural convection) as well as surface-tension-driven flows (Marangoni flows); see Fig. 1.

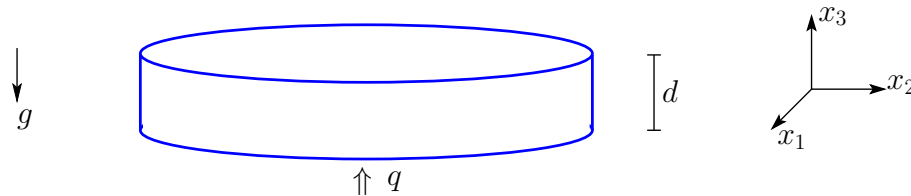


Figure 1: Three-dimensional Bénard-Marangoni convection problem: a fluid layer of thickness d is heated from below. Gravity is pointing downwards. The bottom surface represents a fixed wall kept at a constant temperature T_0 . The top surface represents a free surface which may be deformed.

This problem represents a coupled thermal fluid problem. The governing equations are given by the conservation of mass, linear momentum and energy.

Buoyancy-driven flow is due to the fact that the density, ρ , is a function of the temperature, T , something which gives rise to a volumetric body force in the presence of temperature gradients. Surface-tension-driven flow is due to the fact that the surface tension, γ , is a function of the temperature, something which gives rise to surface forces (or thermocapillary forces) along the free surface in the presence of temperature gradients.

We will assume the following linearizations:

$$\rho(T) = \rho_0(1 - \beta(T - T_0)), \quad (2.1)$$

$$\gamma(T) = \gamma_0(1 - \tau(T - T_0)). \quad (2.2)$$

Here, ρ_0 and γ_0 represent the reference values of the density and the surface tension at the temperature T_0 , while β and τ are constants (typically positive). The temperature $T = T_0$ will be imposed on the bottom surface.

At the top surface, we assume that, in the absence of convection, the temperature is held at a constant value $T = T_1$. We also assume that the temperature T in the domain can

be expressed as

$$T(x_1, x_2, x_3, t) = T_0 - \frac{\Delta T}{d} x_3 + \Theta(x_1, x_2, x_3, t), \quad (2.3)$$

where $\Delta T = T_0 - T_1 > 0$ is the positive temperature difference between the bottom and the top surface in the purely conductive regime, d is the distance between the top and bottom surfaces, and Θ represents the deviation in the temperature from a purely linear temperature profile. In the following, we assume that $\Theta = 0$ at the bottom surface, while $\frac{\partial \Theta}{\partial n} = 0$ at the top surface.

A couple of remarks are in order at this point. First, with the onset of convection, we expect Θ to be nonzero at the surface; in particular, we expect the surface gradient of Θ to be nonzero. The implication of this is that the temperature T is no longer exactly equal to T_1 at the top surface as it is in the purely conductive regime. Second, experiments have shown that the top surface becomes slightly deformed with the onset of convection. This means that the normal derivative along the top surface does not exactly correspond to the derivative with respect to x_3 . We will account for a potential surface deformation in our mathematical model and in our simulations.

The governing equations for the fluid velocity, the pressure and the temperature can be expressed as (the Boussinesq approximation):

$$\frac{\partial u_j}{\partial x_j} = 0, \quad \text{in } \Omega, \quad (2.4)$$

$$\rho_0 \left(\frac{\partial u_i}{\partial t} + u_j \frac{\partial u_i}{\partial x_j} \right) = \frac{\partial \sigma_{ij}}{\partial x_j} - \rho(T) g \delta_{i3}, \quad \text{in } \Omega, \quad i = 1, 2, 3, \quad (2.5)$$

$$\rho_0 c \left(\frac{\partial T}{\partial t} + u_j \frac{\partial T}{\partial x_j} \right) = k \frac{\partial^2 T}{\partial x_j \partial x_j}, \quad \text{in } \Omega. \quad (2.6)$$

Here, u_i is the i -th component of the fluid velocity in an inertial reference frame, x_j is the j -th coordinate, g is gravity (a positive constant), c represents the specific heat capacity, k is the thermal conductivity, and δ is the Kronecker delta symbol. Summation over repeated indices is assumed. The stress tensor σ_{ij} for a viscous Newtonian fluid is given as

$$\sigma_{ij} = -p \delta_{ij} + \mu \left(\frac{\partial u_i}{\partial x_j} + \frac{\partial u_j}{\partial x_i} \right), \quad i, j = 1, 2, 3, \quad (2.7)$$

where p is the pressure and μ is the dynamic viscosity.

We remark that the fluid is modelled as an incompressible fluid, but with a buoyancy term (volumetric body force) arising from small density variations following (2.1). The fluid flow is also coupled to the temperature via the surface tension; see (2.2). The temperature is coupled to the fluid flow via the convection term in (2.6).

The domain Ω represents the fluid layer. The top and bottom surfaces of this domain will be denoted as $\partial\Omega_t$ and $\partial\Omega_b$, respectively. The vertical side wall(s) will be denoted as $\partial\Omega_s$. This can be a single cylindrical wall as depicted in Fig. 1, however, we will later also consider domains with polygonal cross-sections.

2.1 Boundary conditions

We now discuss the boundary conditions. We assume that the bottom surface and the vertical side walls are rigid. Hence, along $\partial\Omega_b$ and $\partial\Omega_s$ we impose homogeneous Dirichlet boundary conditions for the velocity,

$$u_i = 0, \quad \text{on } \overline{\partial\Omega_b} \cup \overline{\partial\Omega_s}, \quad i = 1, 2, 3.$$

Along the top surface $\partial\Omega_t$ we impose free surface boundary conditions. Both for the mathematical and numerical treatment of these boundary conditions it will prove highly advantageous to express these conditions using surface-intrinsic coordinates. However, before giving the expressions, we first introduce some necessary notation and definitions from differential geometry [9, 15, 26].

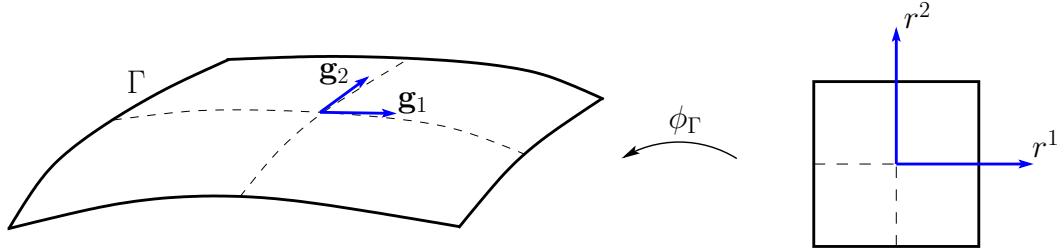


Figure 2: A plot depicting part of a deformed surface Γ in three dimensions. We assume that there exist a parameterization of this surface patch using two independent coordinates. In particular, we can describe the surface patch through a one-to-one mapping of an undeformed square. From this surface parameterization, we can define covariant base vectors \mathbf{g}_1 and \mathbf{g}_2 at any point on the surface. These vectors will span the tangent plane, but will generally not be orthogonal or of unit length.

Consider the surface patch Γ depicted in Fig. 2. We assume that a point \mathbf{x} on Γ has coordinates given through the parameterization $x_i = x_i(r^1, r^2)$, $i = 1, 2, 3$, with $-1 \leq r^1, r^2 \leq 1$. The following results from differential geometry will then prove useful:

$$\mathbf{g}_\alpha = \frac{\partial \mathbf{x}}{\partial r^\alpha}, \quad \alpha = 1, 2, \quad (2.8)$$

$$\mathbf{g}_\alpha \cdot \mathbf{g}_\beta = g_{\alpha\beta}, \quad \alpha = 1, 2, \quad \beta = 1, 2, \quad (2.9)$$

$$g_{\alpha k} g^{k\beta} = \delta_\alpha^\beta, \quad (2.10)$$

$$\mathbf{g}^\alpha = g^{\alpha\beta} \mathbf{g}_\beta, \quad (2.11)$$

$$g = \sqrt{\det(g_{\alpha\beta})}. \quad (2.12)$$

Here, the vectors \mathbf{g}_α represent the covariant base vectors, while the vectors \mathbf{g}^α represent the contravariant base vectors. Both sets of vectors span the tangent plane, and the two sets are mutually orthogonal ($\mathbf{g}_\alpha \cdot \mathbf{g}^\beta = \delta_{\alpha\beta}$).

The free surface boundary conditions along a surface patch Γ can then be expressed

as [15, 16]

$$n_i \sigma_{ij} n_j = \gamma \kappa, \quad (2.13)$$

$$t_i \sigma_{ij} n_j = t_i \left(g_i^\alpha \frac{\partial \gamma}{\partial r^\alpha} \right). \quad (2.14)$$

Here, κ is twice the mean curvature, n_i , $i = 1, 2, 3$, is the outward unit normal on the surface, and t_i , $i = 1, 2, 3$, represents any tangent vector on the surface. We remark that the quantity $(g_i^\alpha \frac{\partial \gamma}{\partial r^\alpha})$ represents the i th component of the surface gradient of the surface tension, or equivalently, the tangential surface forces in the i th direction. Note that, with no loss in generality, we have assumed an atmospheric pressure equal to zero in (2.13).

Since the surface tension depends on the co-ordinates indirectly via the temperature, the tangential boundary conditions can also be expressed as

$$t_i \sigma_{ij} n_j = -t_i \left(g_i^\alpha \frac{\partial T}{\partial r^\alpha} \gamma_0 \tau \right). \quad (2.15)$$

Note that the derivative $\frac{d\gamma}{dT} = -\gamma_0 \tau$ according to our linearization (2.2).

2.2 Treatment of the pressure

Before we express the governing equations in non-dimensional form, we discuss the treatment of the pressure. In the momentum equations, we express the buoyancy term on the right hand side as

$$\rho_0 g \delta_{i3} (1 - \beta(T - T_0)) = \rho_0 g \delta_{i3} + \rho_0 g_i \delta_{i3} \beta \frac{\Delta T}{d} x_3 - \rho_0 g \delta_{i3} \beta \Theta.$$

The first two terms on the right hand side can again be expressed as

$$\rho_0 g \delta_{i3} + \rho_0 g \delta_{i3} \beta \frac{\Delta T}{d} x_3 = \frac{\partial}{\partial x_3} \left(\rho_0 g x_3 + \frac{1}{2} \rho_0 g \beta \frac{\Delta T}{d} x_3^2 \right) \delta_{i3}.$$

Hence, these two terms can be "absorbed" into the pressure by defining a modified pressure

$$p^*(x_1, x_2, x_3, t) = p(x_1, x_2, x_3, t) + \rho_0 g x_3 + \frac{1}{2} \rho_0 g \beta \frac{\Delta T}{d} x_3^2.$$

The meaning of this is just that the modified pressure already includes the contribution from the hydrostatic pressure (the term $\rho_0 g x_3$) and the contribution from the buoyancy term associated with a linear temperature profile, $\frac{1}{2} \rho_0 g \beta \frac{\Delta T}{d} x_3^2$. In summary, with the new modified pressure, we can write

$$-\frac{\partial p}{\partial x_i} + \rho_0 g \delta_{i3} (1 - \beta(T - T_0)) = -\frac{\partial p^*}{\partial x_i} + \rho_0 g \delta_{i3} \beta \Theta, \quad i = 1, 2, 3.$$

In the following, we will assume that we do this modification of the pressure and will just drop the superscript *.

2.3 Non-dimensionalization

We now proceed with non-dimensionalizing the governing equations. To this end, we non-dimensionalize the spatial co-ordinates by setting

$$x'_i = x_i/d, \quad i = 1, 2, 3,$$

and scaling time with the thermal diffusion time constant,

$$t' = t/(d^2/\alpha_T),$$

where the thermal diffusivity

$$\alpha_T = k/\rho_0 c.$$

The scaling of length and time naturally gives a scaling for velocity as the ratio $d/(d^2/\alpha_T) = \alpha_T/d$. Hence, we non-dimensionalize the velocity as

$$u'_i = u_i/(\alpha_T/d), \quad i = 1, 2, 3.$$

In addition, it will prove natural to non-dimensionalize the pressure as

$$p' = p/(\mu\alpha_T/d^2).$$

Finally, we scale the temperature using the temperature difference ΔT , i.e.,

$$T' = T/\Delta T.$$

Dropping all the primes, the governing equations in Ω can then be expressed in non-dimensional form as

$$\frac{\partial u_j}{\partial x_j} = 0, \tag{2.16}$$

$$\frac{1}{\text{Pr}} \left(\frac{\partial u_i}{\partial t} + u_j \frac{\partial u_i}{\partial x_j} \right) = -\frac{\partial \sigma_{ij}}{\partial x_j} + \text{Ra} \Theta \delta_{i3}, \quad i = 1, 2, 3, \tag{2.17}$$

$$\frac{\partial \Theta}{\partial t} + u_j \frac{\partial \Theta}{\partial x_j} = \frac{\partial^2 \Theta}{\partial x_j \partial x_j} + u_3. \tag{2.18}$$

Here, all the dependent and independent variables should be interpreted as being non-dimensional quantities according to the scalings discussed above. In addition, we have introduced the Prandtl number,

$$\text{Pr} = \frac{\nu}{\alpha_T}$$

where $\nu = \mu/\rho_0$ is the kinematic viscosity, and the Rayleigh number,

$$\text{Ra} = \frac{g\beta\Delta T d^3}{\alpha_T \nu}.$$

We also need to non-dimensionalize the boundary conditions. To this end, we need to use the same scalings as for the governing equations. For the normal direction along the free surface $\partial\Omega_t$ we get

$$n_i\sigma_{ij}n_j = \gamma\kappa, \quad (2.19)$$

where γ is a non-dimensional surface tension given by

$$\gamma(\Theta) = \frac{1}{Ca} + Ma(1 - \Theta), \quad (2.20)$$

and κ is the non-dimensional curvature. Note that γ in (2.20) depends on the non-dimensional temperature Θ , the Capillary number, Ca , defined as

$$Ca = \frac{\mu\alpha_T}{\gamma_0 d},$$

and the Marangoni number, Ma , defined as

$$Ma = \frac{\gamma_0 \tau \Delta T d}{\mu\alpha_T}.$$

For the tangent direction along the free surface, we get

$$t_i\sigma_{ij}n_j = Ma \left(t_i g_i^\alpha \frac{\partial}{\partial r^\alpha} (1 - \Theta) \right). \quad (2.21)$$

The components of the non-dimensional stress tensor are given as

$$\sigma_{ij} = -p\delta_{ij} + \left(\frac{\partial u_i}{\partial x_j} + \frac{\partial u_j}{\partial x_i} \right), \quad i, j = 1, 2, 3,$$

where p and u_i , $i = 1, 2, 3$ represent the non-dimensional pressure and nondimensional velocity, respectively.

The remaining boundary conditions are:

$$\frac{\partial \Theta}{\partial n} = 0, \quad \text{on } \partial\Omega_t, \quad (2.22)$$

$$\frac{\partial \Theta}{\partial n} = 0 \quad \text{and} \quad u_i = 0, \quad i = 1, 2, 3, \quad \text{on } \partial\Omega_s, \quad (2.23)$$

$$\Theta = 0 \quad \text{and} \quad u_i = 0, \quad i = 1, 2, 3, \quad \text{on } \partial\Omega_b. \quad (2.24)$$

Finally, we need to specify initial conditions for the temperature and the velocity.

3 Governing equations: Weak form

We now present the weak formulation of the non-dimensionalized problem (2.16)-(2.18), subject to the boundary conditions (2.19), (2.21), and (2.22)-(2.24).

We first introduce the function spaces X , Y , and Z defined as

$$\begin{aligned} X &= \{v(t) \in H^1(\Omega(t)), v(t) = 0 \text{ on } \overline{\partial\Omega_b} \cup \overline{\partial\Omega_s}\}, \\ Y &= \{q(t) \in L^2(\Omega(t))\}, \\ Z &= \{v(t) \in H^1(\Omega(t)), v(t) = 0 \text{ on } \overline{\partial\Omega_b}\}. \end{aligned}$$

The governing equations for fluid flow can then be expressed as: find $u_i(t) \in X$, $i = 1, 2, 3$ and $p(t) \in Y$ such that

$$\begin{aligned} &\frac{1}{\text{Pr}} \int_{\Omega(t)} \left(v_i \frac{\partial u_i}{\partial t} + v_i u_j \frac{\partial u_i}{\partial x_j} \right) d\Omega \\ &= \int_{\Omega(t)} \left(-\frac{\partial v_i}{\partial x_j} \sigma_{ij} + v_i \text{Ra} \Theta \delta_{i3} \right) d\Omega + I_\gamma(v_i), \quad \forall v_i(t) \in X, \end{aligned} \quad (3.1)$$

$$\int_{\Omega(t)} q \frac{\partial u_j}{\partial x_j} d\Omega = 0, \quad \forall q(t) \in Y, \quad (3.2)$$

while the governing equation for heat transfer can be expressed as: find $\Theta(t) \in Z$ such that

$$\int_{\Omega(t)} \left(v \frac{\partial \Theta}{\partial t} + v u_j \frac{\partial \Theta}{\partial x_j} \right) d\Omega = \int_{\Omega(t)} \left(-\frac{\partial v}{\partial x_j} \frac{\partial \Theta}{\partial x_j} + v u_3 \right) d\Omega, \quad \forall v(t) \in Z. \quad (3.3)$$

Note that we have here explicitly indicated that the (non-dimensional) domain Ω can be a function of time. In (3.1),

$$I_\gamma(v_i) = \int_{\partial\Omega_\gamma(t)} v_i \sigma_{ij} n_j dS \quad (3.4)$$

is the surface integral resulting from integration by parts of the volume term $\int_{\Omega(t)} v_i \frac{\partial \sigma_{ij}}{\partial x_j} d\Omega$. Using the boundary conditions (2.19) and (2.21) we can express this integral as

$$I_\gamma(v_i) = \int_{\partial\Omega_\gamma(t)} v_i \left(\gamma(\Theta) \kappa n_i + \text{Ma} \left(g_i^\alpha \frac{\partial}{\partial r^\alpha} (1 - \Theta) \right) \right) dS \quad (3.5)$$

The curvature-normal product κn_i can again be replaced with a very powerful expression presented in [12] and derived in detail in [3],

$$\kappa n_i = \frac{1}{g} \frac{\partial (g g_i^\alpha)}{\partial r^\alpha}, \quad (3.6)$$

where g is the square root of the determinant of the metric tensor; see (2.12). Inserting (3.6) into (3.5) and using (2.20) we get

$$I_\gamma(v_i) = \int_{\partial\Omega_\gamma(t)} v_i \left[\left(\frac{1}{\text{Ca}} + \text{Ma}(1-\Theta) \right) \frac{1}{g} \frac{\partial(gg_i^\alpha)}{\partial r^\alpha} + \text{Ma} \left(g_i^\alpha \frac{\partial}{\partial r^\alpha} (1-\Theta) \right) \right] dS. \quad (3.7)$$

Using integration by parts on the integral in (3.7) and simplifying the expressions, we readily arrive at the following simple expression for the surface integral $I_\gamma(v_i)$,

$$I_\gamma(v_i) = - \int_{\partial\Omega_\gamma(t)} \gamma(\Theta) \frac{\partial v_i}{\partial r^\alpha} g_i^\alpha dS. \quad (3.8)$$

We now make several remarks regarding the final form (3.8). First, we have here assumed that we do not get any contribution from the boundary of the free surface (i.e., the surface of the free surface) when we perform the second integration by parts. This assumption is satisfied when the free surface is attached to a wall ($v_i=0$), for periodic boundary conditions (which we will also consider below), and for free surfaces with no boundaries at all (e.g., for bubbles). Second, the simple form (3.8) is the same as presented in [12], and we will here exploit this form in order to simulate three-dimensional Bénard-Marangoni flows. To our knowledge, this is the first time this variational form has been exploited for such problems, and where also free surface deformations are allowed. Third, this simple expression includes the contribution from *both* normal and tangential stresses; the integrand has a form similar to a surface Laplacian and allows for a variable surface tension. Note that no differentiation of the surface tension is required. Another advantage of this form comes from the fact that the regularity requirement on the geometry representation has been lowered through integration-by-parts; only the first derivative of x_i is necessary even though this expression also incorporates curvature effects.

4 ALE formulation

Let us now briefly recall the main ingredients in deriving the Arbitrary Lagrangian Eulerian formulation [13] from (3.1)-(3.3). First, we introduce a domain velocity with components w_i , $i=1,2,3$, in order to describe the time-dependent evolution of the domain $\Omega(t)$ both in the interior and on the boundary, i.e.,

$$\frac{dx_i}{dt} = w_i, \quad i=1,2,3.$$

Second, we can exploit Reynolds transport theorem [1] in order to move the differentiation with respect to time outside the volume integral; this will prove very useful for the subsequent numerical treatment since Ω is, in general, time-dependent. Finally, we exploit Euler's expansion formula [1] to arrive at the following ALE-formulation of fluid

problem (3.1)-(3.2): find $u_i(t) \in X, i=1,2,3$ and $p(t) \in Y$ such that

$$\begin{aligned} \frac{1}{\text{Pr}} \frac{d}{dt} \int_{\Omega(t)} v_i u_i d\Omega &= \int_{\Omega(t)} \left(-\frac{\partial v_i}{\partial x_j} \sigma_{ij} + v_i \text{Ra} \Theta \delta_{i3} \right) d\Omega + I_\gamma(v_i) \\ &\quad - \frac{1}{\text{Pr}} \int_{\Omega(t)} \left(v_i [u_j - w_j] \frac{\partial u_i}{\partial x_j} - v_i u_i \frac{\partial w_j}{\partial x_j} \right) d\Omega, \quad \forall v_i(t) \in X, \end{aligned} \tag{4.1}$$

$$\int_{\Omega(t)} q \frac{\partial u_j}{\partial x_j} d\Omega = 0, \quad \forall q(t) \in Y. \tag{4.2}$$

The ALE-formulation of the heat transfer problem (3.3) reads: find $\Theta(t) \in Z$ such that

$$\begin{aligned} \frac{d}{dt} \int_{\Omega(t)} v \Theta d\Omega &= \int_{\Omega(t)} \left(-\frac{\partial v}{\partial x_j} \frac{\partial \Theta}{\partial x_j} + v u_3 \right) d\Omega \\ &\quad - \int_{\Omega(t)} \left(v [u_j - w_j] \frac{\partial \Theta}{\partial x_j} - v \Theta \frac{\partial w_j}{\partial x_j} \right) d\Omega, \quad \forall v(t) \in Z. \end{aligned} \tag{4.3}$$

We remark that the last integrals in (4.1) and (4.3) represent all the convective contributions.

In addition, we must also impose a kinematic condition along the free surface $\partial\Omega_t(t)$:

$$w_j n_j = u_j n_j. \tag{4.4}$$

This condition says that the normal velocity of the free surface must coincide with the normal fluid velocity along the free surface ("fronttracking"). No particular condition is required for the tangential domain velocity, and this flexibility can be exploited when considering the subsequent numerical treatment. There is also significant flexibility in terms of the extension of the domain velocity from the boundary to the interior; see [10].

Finally, we need to impose initial conditions for the temperature and the velocity.

5 Discretization

Our starting point for the numerical discretization is the ALE formulation presented above. The domain $\Omega(t)$ is first decomposed into K spectral elements, $\Omega^k, k=1, \dots, K$; see [17]. Each element Ω^k is considered as a unique mapping Φ^k of the reference domain $\hat{\Omega} = (-1,1)^3$; in the following, the reference variables are denoted as $r^\alpha, \alpha=1,2,3$.

Following this spatial discretization procedure, the fluid velocity, the temperature, the mesh velocity, and the geometry are all approximated as N th order polynomials in each spatial direction in each element (all expressed in terms of the reference variables $r^\alpha, \alpha=1,2,3$), while the pressure is approximated as polynomials of degree $N-2$ within each element. The discrete problem derived through a Galerkin procedure then represents a stable discretization and results in a spatial discretization error which depends on the regularity of the solution and the data; see [17].

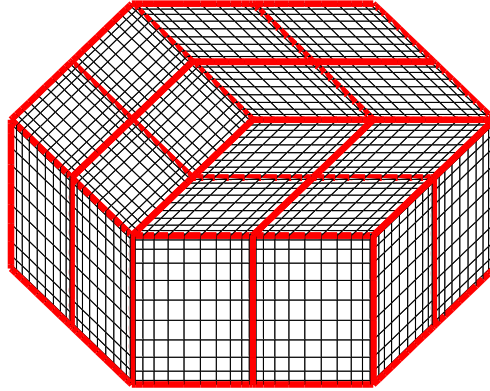


Figure 3: Spectral element grid for the simulation of Bénard-Marangoni convection in a three-dimensional "cylinder"; the cross-section is here a six-sided polygon. The domain is decomposed into a single layer of $K=12$ spectral elements, each of order N . The free surface (top surface) is here comprised of twelve element faces, with each face representing a surface patch Γ as discussed earlier; see Fig. 2.

The spectral element method has previously been used to simulate three-dimensional, viscous, free surface flows [5, 12], however, the more general case involving Bénard-Marangoni flows with deformable free surfaces has not been considered before using any computational method. In the rest of this section we thus focus on the geometry representation and on how this is used to incorporate the general free surface boundary conditions discussed earlier.

Consider for a moment the geometry representation within element Ω^k . We express the physical coordinates using a nodal, tensor-product basis,

$$x_i^{k,N}(r^1, r^2, r^3) = \sum_{l=0}^N \sum_{m=0}^N \sum_{n=0}^N (x_i^{k,N})_{lmn} \ell_l(r^1) \ell_m(r^2) \ell_n(r^3), \quad i=1,2,3, \quad (5.1)$$

where $(x_i^{k,N})_{lmn}$ are the basis coefficients (nodal values), and $\ell_p(r) \in \mathbb{P}_N(-1,1)$ is the one-dimensional Lagrangian interpolant through the Gauss-Lobatto Legendre points ξ_q , $q=0, \dots, N$, and with

$$\ell_p(\xi_q) = \delta_{pq}.$$

A common procedure to determine the nodal values $(x_i^{k,N})_{lmn}$ is to first determine the surface values from known data, and then compute the interior values via a Gordon-Hall mapping procedure [8, 11]. It should be clear from (5.1) that, since the geometry is also approximated as N th order polynomials, we are using an isoparametric representation.

The free surface boundary conditions are imposed through the surface integral given in (3.8). Let us briefly discuss the details of how this is done for the discrete problem. First, we remark that the free surface will comprise a number of element faces. For example, in Fig. 3, the free surface (top surface) is comprised of 12 element faces. Let us assume that the free surface representation corresponding to element Ω^k is given by (5.1) for $r^3=1$. In this case, the surface patch depicted in Fig. 2 is simply given by $x_i^{k,N}(r^1, r^2, 1)$.

Hence, we automatically have a parameterization of each surface patch. Applying (2.8) to this surface parameterization, we can easily construct the covariant base vectors \mathbf{g}_α through simple differentiation. At this point, the metric tensors, contravariant base vectors etc. can easily be computed from (2.9)-(2.12).

In the discrete problem the surface integral (3.8) is first broken up into a sum of smaller integrals, each integral going over one single element face (or surface patch). Each such integral is again expressed in terms of the reference variables (e.g., r^1 and r^2), and a standard Gauss-Lobatto Legendre quadrature rule is used. Note that the differential dS in (3.8) should be expressed as

$$dS = g \, dr^1 \, dr^2$$

before Gauss quadrature is employed.

For the temporal discretization we have extended the convection-Stokes splitting approach presented in [18] (the OIF-method) to time-dependent geometries. This has allowed us to obtain first, second or third order convergence in time for selected problems; see the following section for a numerical test problem. We remark that the work presented in this paper is part of a larger research effort on high-order methods for problems in time-dependent domains, and the technical details of the temporal treatment will be reported elsewhere. The applications we focus on in this paper represent steady state solutions, however, each discrete approximation is obtained by integrating the unsteady equations until a steady state has been reached.

6 Numerical test problem

We first verify our discretization approach by solving the three-dimensional Navier-Stokes equations in a cylindrical domain as depicted in Fig. 4. The domain boundary is here fixed at all times, however, we specify an artificial time-periodic mesh velocity in the interior. The mesh velocity is a function of both space and time, and is zero on the domain boundary; see Fig. 5. In fact, the mesh velocity is chosen to be C^∞ within each spectral element, but only C^0 across the element boundaries. We also specify a forcing function in the momentum equations by requiring that the following analytic solution satisfies the incompressible Navier-Stokes equations (here expressed in cylindrical coordinates):

$$u_r(r, \theta, z, t) = \frac{1}{5} \sin^2(\pi r) \sin(\theta) \sin(2\pi z) \sin(t), \quad (6.1)$$

$$u_\theta(r, \theta, z, t) = -\frac{1}{5} \sin^2(\pi r) \cos(\theta) \sin(2\pi z) \sin(t), \quad (6.2)$$

$$u_z(r, \theta, z, t) = \frac{1}{10\pi} \sin(\pi r) \left(2\pi \cos(\pi r) + \frac{2}{r} \sin(\pi r) \right) \sin(\theta) (\cos(2\pi z) - 1) \sin(t), \quad (6.3)$$

$$p(r, \theta, z, t) = \sin^2(\pi r) \sin(\pi z) \sin(t). \quad (6.4)$$

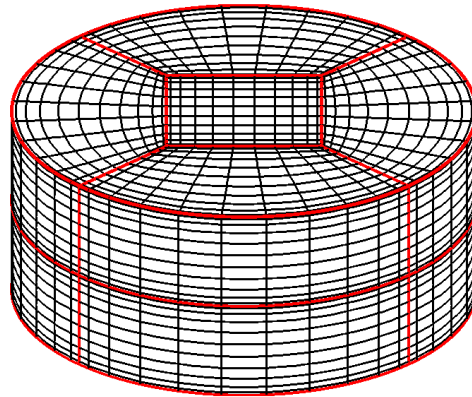


Figure 4: Computational domain used in the convergence study of the ALE scheme. The cylindrical domain is decomposed into two layers of spectral elements, each layer comprising five spectral elements.

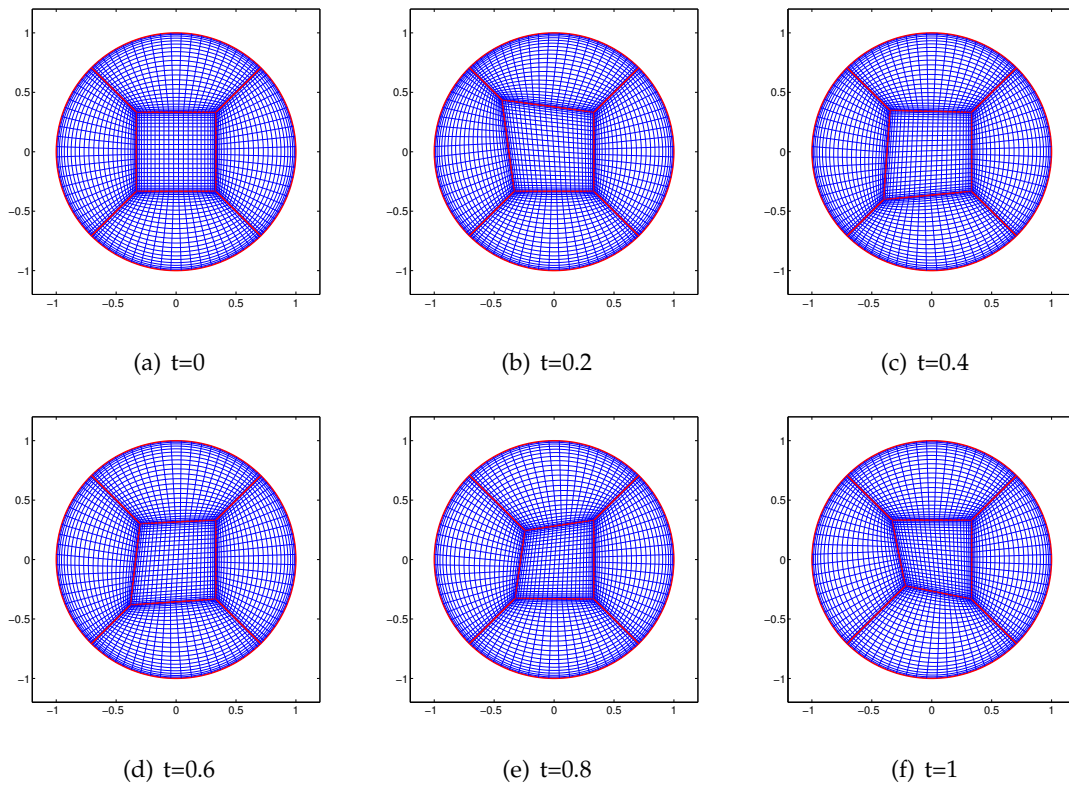


Figure 5: The external boundary of the cylindrical domain in Fig. 4 is fixed. However, we specify a mesh velocity in the interior of the cylinder which is a function of both space and time (periodic in time). The plot shows the grid-configuration at a few time levels of the mid-plane of the cylinder during one single period. The exact flow solution in the cylindrical domain is given by (6.1)-(6.4).

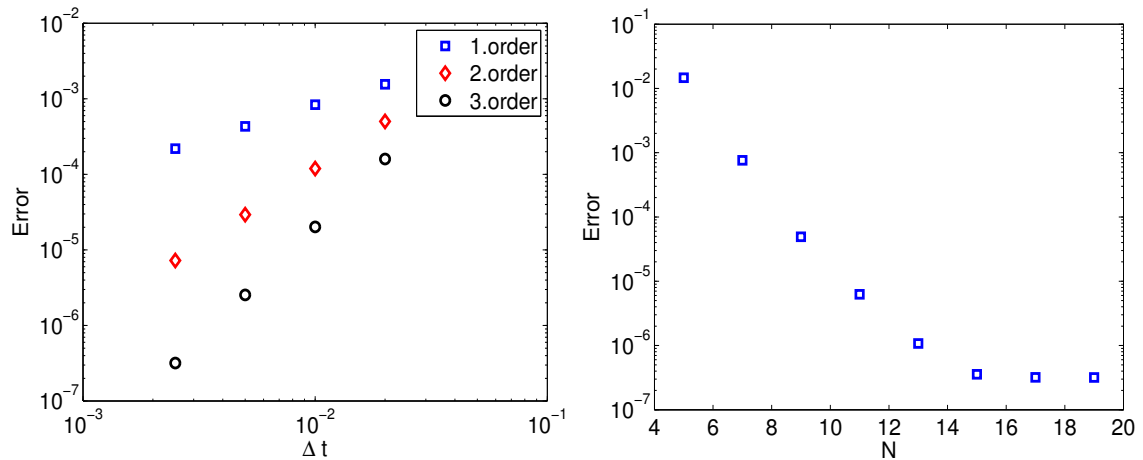


Figure 6: The left plot depicts the discretization error (energy norm) as a function of the time step, Δt , for a first, second, and third order temporal splitting scheme; the spatial error is here subdominant the temporal error. The right plot depicts the discretization error as a function of the polynomial degree, N , used in each spectral element; the temporal error is here subdominant the spatial error for $N < 15$.

The convergence results in Fig. 6 show the expected behavior: first, second, and third order convergence in time, and exponential convergence in space for problems with analytic solutions and data. A complete discussion of the splitting scheme, together with additional numerical results, will be presented in a forthcoming article.

7 Simulation of three-dimensional Bénard-Marangoni flows

We now present simulation results which exploit many benefits of the proposed computational approach. In particular, we consider Bénard-Marangoni convection in a horizontal fluid layer heated from below and with a free surface on the top. The terms "top" and "bottom" here refer to the case when gravitational forces are present (e.g., on Earth with gravity pointing downwards); however, we also consider zero-gravity conditions.

An issue which has been studied extensively, both experimentally and theoretically, is the small deformation of the free surface in the presence of hexagonal cells. Depending on whether buoyancy effects or surface tension gradient effects are dominating, the free surface is either elevated or depressed at the centers of the cells. Previous computational studies of Bénard-Marangoni convection have been done, however, all these studies assume a fixed and undeformed "free" surface. In the present study, we include all the physical effects, combining both normal and tangential stresses along the free surface via the surface integral I_γ . We are therefore able to compute the associated surface deflection over each hexagonal cell.

We now report some of the results obtained by our computational approach. The first results are for the case with an infinite Prandtl number and zero Rayleigh number. In

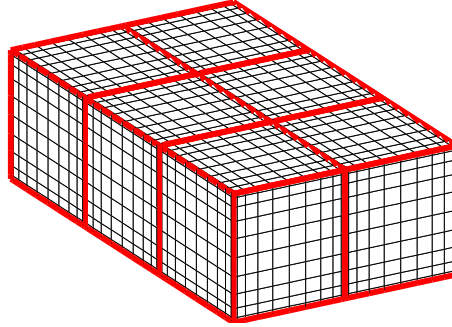


Figure 7: Spectral element grid for the simulation of Bénard-Marangoni convection in a three-dimensional box. The domain is decomposed into a single layer of $K=6$ spectral elements, each of order N . The free surface (top surface) is here comprised of six element faces.

steady state, this corresponds to the limit of solving the steady Stokes equations in zero gravity conditions. The computational domain is a three-dimensional box, with periodic boundary conditions specified along the "vertical" sides. This particular case has been studied computationally in [24] and [19], but then with a fixed and flat "free" surface.

The spectral element discretization used to solve this problem is depicted in Fig. 7. Specifically, the physical domain is given by $\Omega = (0, l_x) \times (0, l_y) \times (0, d)$, with

$$\frac{l_x}{d} = \frac{4\pi}{\sqrt{3}k}, \quad \frac{l_y}{d} = \frac{4\pi}{k},$$

and with $k=1.9929$. The specific periodicity lengths are compatible with the formation of a single hexagonal cell as predicted by linear stability theory [7, 14, 21]. These periodicity lengths are also used in [24] and [19].

At this point we comment on the periodic boundary conditions that we impose along the "vertical" sides (periodicity in the x_1 and x_2 directions). Periodic boundary conditions were also used in [24], while [19] imposed symmetry boundary conditions. Both [24] and [19] used the velocity formulation of the Navier-Stokes equations, which is appropriate for this problem as long as a flat and fixed "free" surface is assumed. However, it is interesting to note that symmetry boundary conditions *cannot* be used in our case since we are using the full stress formulation of the Navier-Stokes equations; symmetry boundary conditions (i.e., zero tangential stress) along the "vertical" sides will not be compatible with the free surface boundary conditions for this problem.

Along the free surface, the normal mesh velocity is set equal to the normal fluid velocity in accordance with the kinematic condition (4.4). Homogeneous Dirichlet boundary conditions are chosen for the tangential components, and the interior mesh velocity is computed through a simple element-based Gordon-Hall mapping; see [11]. These choices can certainly be justified for this type of applications where we expect the free surface deformation to be small. Note that, at steady state, the normal fluid velocity is zero along the free surface, and the mesh velocity is zero in the entire domain. Also note

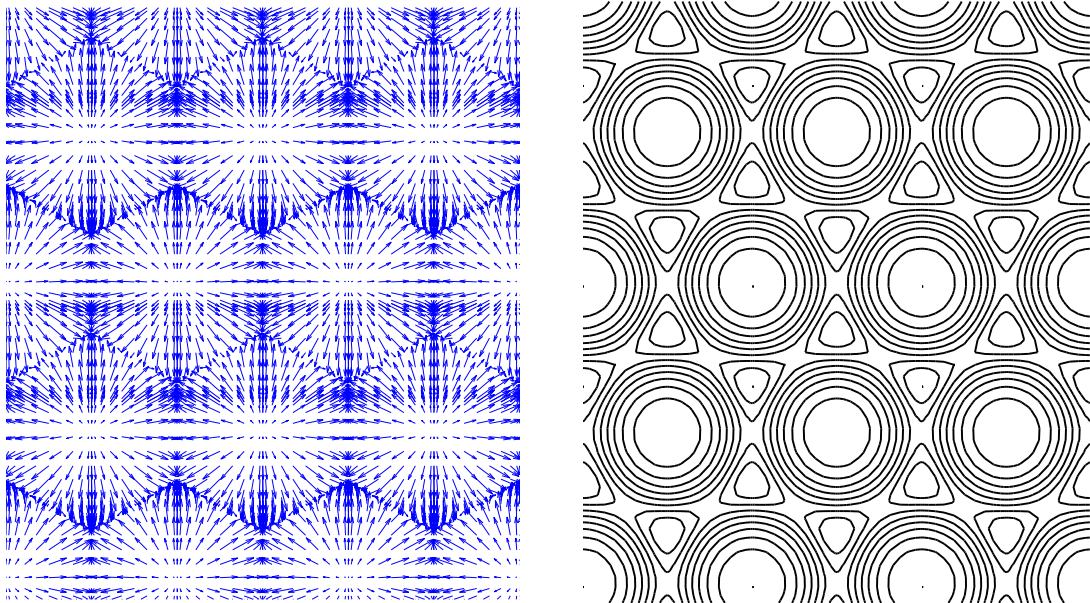


Figure 8: Numerical results for the three-dimensional Bénard-Marangoni convection problem. The left plot shows the velocity vectors, while the right plot depicts the temperature distribution over the free surface at steady state (top view) for the case with $Ma=90$, $Ra=0$, $Pr=\infty$, and $Ca=3\cdot 10^{-4}$.

that, at steady state, the temporal splitting scheme will have steady state errors, similar to the original OIF-scheme for fixed geometries; see [18].

The initial condition for the velocity is zero, while the temperature (or, more precisely, the deviation from a purely conductive temperature profile) is set to be a random field at time $t=0$. Specifically, we set

$$\Theta(x_1, x_2, x_3, t=0) = \Theta_0 \cdot \text{Rand}(x_1, x_2) \cdot x_3(2 - x_3),$$

with $\Theta_0=0.1$, and $\text{Rand}(x_1, x_2)$ a random variable in the $[0,1]$ range.

We first present numerical results for $Ma=90$. The results in Fig. 8 depict the velocity vectors and temperature distribution over the free surface at steady state (top view); we clearly see the presence of hexagonal cells. The center of each cell is hot, while the exterior region of each cell is cold. In Fig. 9 we also show the deformation of the free surface over a single cell; the depressed free surface at the center of the cell is consistent with the fact that there are no buoyancy effects. Fig. 10 illustrates the same results seen from above (using a different shading to represent surface elevation); we clearly see that the results are independent of the particular surface discretization, indicating the advantages of expressing the surface integral I_γ in (3.8) using surface intrinsic coordinates. Finally, in Fig. 11, we report the maximum surface deflection as a function of the Capillary number; the results are consistent with earlier theoretical results based on linear stability analysis; see [23].

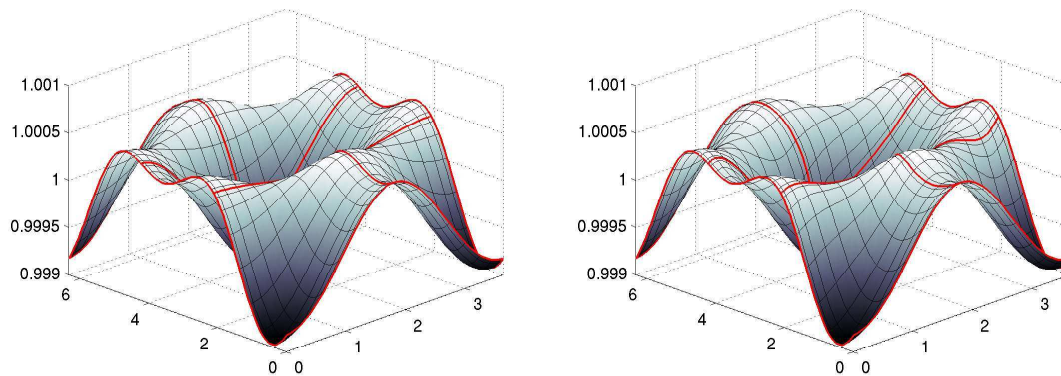


Figure 9: Non-dimensional free surface elevation over a single periodic structure using two different spectral element grids: one grid with straight sides (left) and one grid with deformed sides (right) inside the periodic structure. Here, $Ma=90$, $Ra=0$, $Pr=\infty$, and $Ca=3\cdot 10^{-4}$.

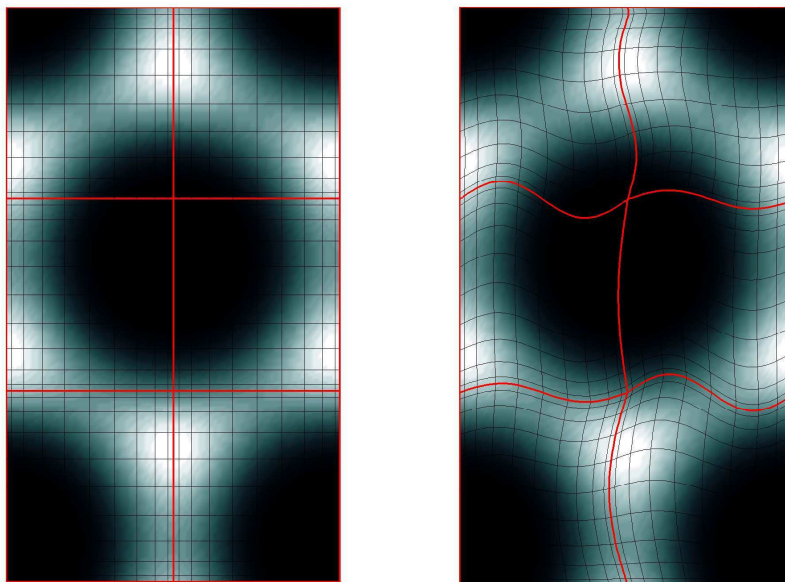


Figure 10: Similar results as in Fig. 9, but now showing the top view. A particular shading is here used to illustrate the free surface elevation. Note that the simulation results do not depend on whether we use a very regular spectral element grid (left plot) or an artificially deformed grid (right plot).

We have also computed the kinetic energy

$$E_u = \frac{1}{2l_x l_y} \int_{\Omega} (u_1^2 + u_2^2 + u_3^2) dV$$

for different values of the Marangoni number and at steady state. For these results we have assumed a fixed free surface in order to be able to compare with earlier presented

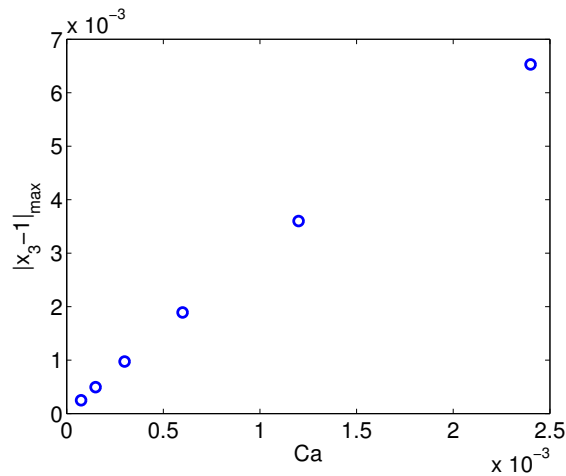


Figure 11: Numerical results for the three-dimensional Bénard-Marangoni convection problem: maximum surface deflection as a function of the Capillary number for the case with $Ma=90$, $Ra=0$, and $Pr=\infty$. Periodic boundary conditions are specified along the "vertical" sides.

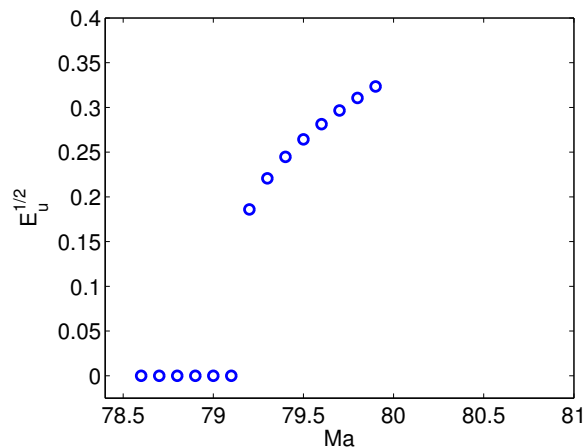


Figure 12: A plot of the energy measure $E_u^{1/2}$ at steady state for different values of the Marangoni number. The domain is the three-dimensional box depicted in Fig. 7.

results. In Fig. 12 we plot $E_u^{1/2}$ as a function of Ma in the range between 78 and 80. Note that we start with the largest Marangoni numbers and reduce Ma until we do not observe any hexagonal cells. From this plot we see that this happens when the Marangoni number $Ma=79.2$. This should be compared with a critical Marangoni number $Ma_c=79.6$ based on linear stability analysis [20]. Our simulation results are in good agreement with the results presented in [24] where the subcritical regime extends down to $Ma=79.0$.

Finally, we show the steady state results for a case where both buoyancy effects and surface gradient effects are present; the particular values of the non-dimensional numbers correspond to the properties of silicon oil. The domain has the shape of a hexagon (top view). The boundary conditions for the fluid problem are solid walls on the bottom

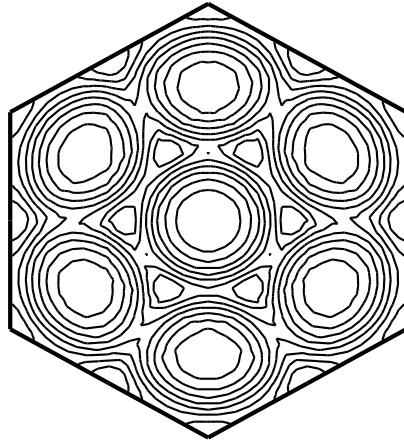


Figure 13: Three-dimensional simulation results for the Bénard-Marangoni convection problem in a hexagonal domain for the case $Ma = 105$, $Ra = 48$, $Pr = 890$, and $Ca = 3 \cdot 10^{-4}$ (corresponding to silicon oil): temperature contours (top view).

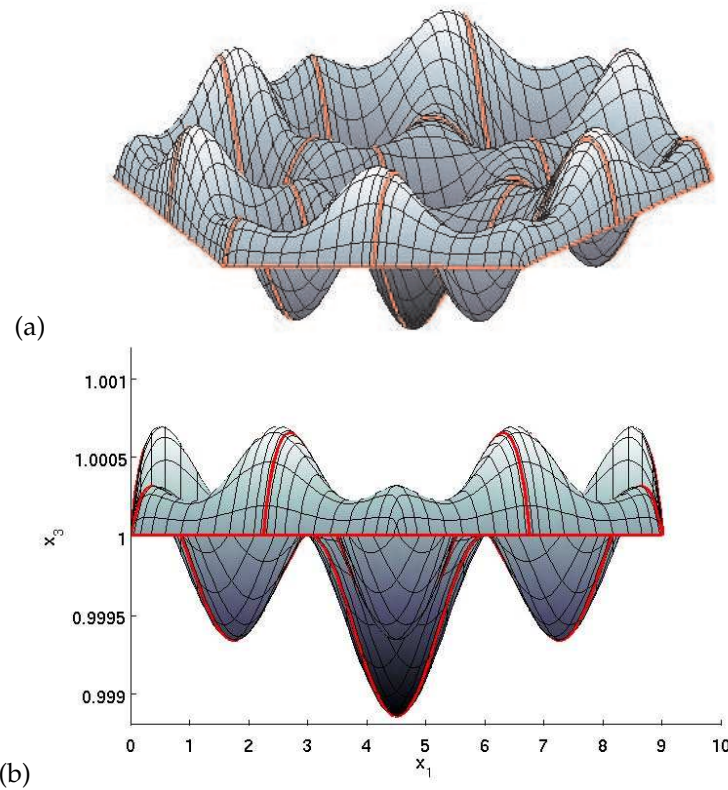


Figure 14: Three-dimensional simulation results for the Bénard-Marangoni convection problem in a hexagonal domain for the case $Ma = 105$, $Ra = 48$, $Pr = 890$, and $Ca = 3 \cdot 10^{-4}$ (corresponding to silicon oil); see Fig. 13: (a) a surface plot of the non-dimensional free surface deflection; (b) side view, including axes. Note that the surface deformation is largest in the center of the domain where the effect of the domain boundary is smallest.

and along the vertical sides, and free surface conditions on the top surface. The boundary conditions for the thermal problem are homogeneous Dirichlet condition on the bottom surface and adiabatic conditions along the remaining sides. The initial condition for the velocity is zero, while the temperature (or, more precisely, the deviation from a purely conductive temperature profile) is again set to be a random field at time $t = 0$. Fig. 13 depicts the temperature contours at steady state, while Fig. 14 depicts the corresponding free surface deflection. The formation of seven cells is in qualitative agreement with the numerical and experimental results presented in [19] using a flat "free" surface. However, we are here also able to predict the detailed free surface deflection.

8 Conclusions

We have presented a coupled thermal-fluid model for Bénard-Marangoni convection in a three-dimensional fluid layer. The governing equations have been derived in a fair amount of detail due to the fact that we have not assumed a flat free surface. In addition, we have presented the free surface boundary conditions (normal and tangential stresses) in general curvilinear coordinates, and thus prepared for the use of flexible discretizations. Based on the weak form of the governing equations, we have presented a high order spatial discretization approach using spectral elements. An operator splitting approach has been used for the temporal treatment. Since we primarily have been interested in steady state solutions, the focus has been on the spatial discretization. The overall computational approach is very attractive to use for several reasons: (i) the solution can be expected to have a high degree of regularity and rapid convergence can be expected; (ii) the spectral element decomposition automatically gives a convenient parameterization of the free surface that allows powerful results from differential geometry to easily be exploited; (iii) free surface deformation can easily be included; (iv) both normal and tangential stresses are conveniently accounted for through a single surface integral; (v) no differentiation of the surface tension is necessary to include thermocapillary effects (due to integration-by-parts twice); (vi) the geometry representation of the free surface need only be C^0 even though curvature effects are included. The proposed approach has been used to simulate Marangoni flows at zero-gravity conditions and at infinite Prandtl number. Finally, we have presented simulation results of Bénard-Marangoni convection in silicon oil. All the results we have obtained are in good agreement with previously reported computational results. However, we are here also able to predict the free surface deflection due to buoyancy and thermocapillary effects; these results are in qualitative agreement with previous experimental and analytical results.

Acknowledgments

The authors would like to thank the Norwegian University of Science and Technology for the financial support of this project.

References

- [1] R. Aris. *Vectors, Tensors, and the Basic Equations of Fluid Mechanics*. Dover Publications, Inc., 1962.
- [2] H. Bénard. Les tourbillons cellulaires dans une nappe liquide transportant de la chaleur par convection en régime permanent. *Annales de Chimie et de Physique*, 23:62–144, 1901.
- [3] T. Bjøntegaard. Imposing free-surface boundary conditions using surface intrinsic coordinates. <http://www.math.ntnu.no/preprint/numerics/2007/N5-2007.pdf>, Technical report, Norwegian University of Science and Technology, 2007.
- [4] M. J. Block. Surface tension as the cause of Bénard cells and surface deformation in a liquid film. *Nature*, 178:650–651, 1956.
- [5] N. Bodard, R. Bouffanais, and M.O. Deville. Solution of moving-boundary problems by the spectral element method. *Applied Numerical Mathematics* (2007). doi:10.1016/j.apnum.2007.04.009, 2007.
- [6] P. Cerisier, C. Jamond, J. Pantaloni, and J. C. Charmet. Déformation de la surface libre en convection de Bénard-Marangoni. *J. Physique*, 45:405–411, 1984.
- [7] S. Chandrasekhar. *Hydrodynamic and Hydromagnetic Stability*. Dover Publications, Inc., 1961.
- [8] M.O. Deville, P.F. Fischer, and E.H. Mund. *High-Order Methods for Incompressible Fluid Flow*. Cambridge University Press, 2002.
- [9] W. Flügge. *Tensor Analysis and Continuum Mechanics*. Springer, Berlin, 1972.
- [10] L. Formaggia and F. Nobile. Stability analysis of second-order time accurate schemes for ALE-FEM. *Computer Methods in Applied Mechanics and Engineering*, 193:4097–4116, 2004.
- [11] W.J. Gordon and C.A. Hall. Construction of curvilinear co-ordinate systems and applications to mesh generation. *International Journal for Numerical Methods in Engineering*, 7:461–477, 1973.
- [12] L.W. Ho and A.T. Patera. Variational formulation of three-dimensional viscous free-surface flows: Natural imposition of surface tension boundary conditions. *International Journal for Numerical Methods in Fluids*, 13:691–698, 1991.
- [13] A. Huerta and A. Rodríguez-Ferran (eds.). The Arbitrary Lagrangian-Eulerian Formulation. *Computer Methods in Applied Mechanics and Engineering*, 193(39-41):4073–4456, 2004.
- [14] E. L. Koschmieder. *Bénard Cells and Taylor Vortices*. Cambridge University Press, 1993.
- [15] E. Kreyszig. *Differential Geometry*. Dover Publications, Inc., 1991.
- [16] L.D. Landau and E.M. Lifshitz. *Fluid Mechanics*. Course of Theoretical Physics, Volume 6. Butterworth-Heinemann, 1987.
- [17] Y. Maday and A.T. Patera. Spectral element methods for the Navier-Stokes equations. in: A.K. Noor, J. T. Oden (Eds.), *State of the Art Surveys in Computational Mechanics*, ASME, New York, pages 71–143, 1989.
- [18] Y. Maday, A.T. Patera, and E.M. Rønquist. An operator-integration-factor splitting method for time-dependent problems: Application to incompressible fluid flow. *Journal of Scientific Computing*, 5(4):263–292, 1990.
- [19] M. Medale and P. Cerisier. Numerical simulation of Bénard-Marangoni convection in small aspect ratio containers. *Numerical Heat Transfer, Part A*, 42:55–72, 2002.
- [20] D.A. Nield. Surface tension and buoyancy effects in cellular convection. *Journal of Fluid Mechanics*, 19:341–352, 1964.
- [21] J.R.A. Pearson. On convection cells induced by surface tension. *Journal of Fluid Mechanics*, 4:489–500, 1958.
- [22] Lord Rayleigh. On convection currents in a horizontal layer of fluid when the higher tem-

- perature is on the under side. *Phil. Mag.*, 32:529–546, 1916.
- [23] L.E. Scriven and C.V. Sternling. On cellular convection driven by surface-tension gradients: effects of mean surface tension and surface viscosity. *Journal of Fluid Mechanics*, 19:321–340, 1964.
- [24] A. Thess and S.A. Orszag. Surface-tension-driven Bénard convection at infinite Prandtl number. *Journal of Fluid Mechanics*, 283:201–230, 1995.
- [25] M. Van Dyke. *An Album of Fluid Motion*. Parabolic Press, Stanford, Ca., 1982.
- [26] C.E. Weatherburn. *Differential Geometry of Three Dimensions*. Cambridge University Press, 1927.